Egg-shell membrane mimicking synthetic polymer membrane supported palladium nanoparticles for catalyzing reduction of uranyl(VI) ions

Sankararao Chappa [a,b], Amol M. Mhatre [a], Vijayalaxmi C. Adya [a], Ashok K. Pandey [a,b,*]

[a] Radiochemistry Division, Bhabha Atomic Research Centre, Trombay, Mumbai 400 085, India
[b] Homi Bhabha National Institute, Training School Complex, Anushaktinagar, Mumbai 400 094, India

ABSTRACT

To develop an efficient, robust and recyclable heterogeneous catalyst, the palladium nanoparticles (Pd NPs) were formed by spontaneous reduction of Pd^{2+} ions with hydrazine covalently attached via glycidyl units to the pore wall of poly(propylene) membrane. After the formation of Pd NPs, the hydrazine grafted membrane was characterized for porosity, through-pores distribution, basicity, elemental mapping and Pd NPs sizes and distribution in the matrix. It was observed that there was a significant reduction of UO_2^{2+} ions by formic acid in the presence of Pd embedded hydrazine grafted membrane; but no reduction of UO_2^{2+} ions by formic acid was observed in the presence of Pd NPs embedded cation-exchange membrane under similar conditions. The analyses of kinetics of reduction of UO_2^{2+} ions by formic acid revealed a threshold amount of Pd^0 in the hydrazine grafted membrane above which reduction occurred in a significant rate. It was observed that kinetic of reduction at lower amount of Pd^0 was controlled by pseudo-second-order kinetics. On increased amount of Pd^0, the reduction process switched to diffusion controlled indicating matrix effect on the reduction kinetics. Therefore, the high intensity ultrasonication was used to overcome the diffusion barrier affecting the kinetics of UO_2^{2+} ions reduction in the Pd NPs embedded neutral membrane matrix. This resulted in a switching of kinetic of the reduction from diffusion controlled process to pseudo-first-order kinetics leading to very high catalytic activity of Pd NPs. The catalytic activity of Pd NPs in the hydrazine grafted poly(propylene) membrane samples did not deteriorate during the five cycles, and after storing for three months suggesting a long shelf-life.

© 2016 Elsevier B.V. All rights reserved.

1. Introduction

Redox chemistry of inorganic ions is important for the applications such as water treatment, remediation of toxic oxidation state of ions, synthetic chemistry of metal complexes having desirable oxidation state, process chemistry, sensor and many other technological applications [1–6]. The aromatic pollutants generated by chemical industries have become serious environmental problem that could be addressed by the catalytic reductions of these aromatic compounds using metal-based catalysts hosted on inorganic or polymer supports [7,8]. It is important to note that the redox reactions of oxyions are not easily feasible under ambient conditions. One of such example is a reduction of UO_2^{2+} ions to U^{4+} ions. The production of U^{4+} ions is required for various applications in the nuclear industries such as stripping of Pu^{4+} ions in PUREX process using U^{4+} ions as reductant without contaminating feed, preparation of UO_2 and UF_4, and so on [6,7]. U^{4+} ions can be easily precipitated at basic pH as UO_2 for its removal and remediation [9]. Due to outermost f electrons, uranium complexes may catalyze the reactions that are normally impossible with the widely used transition-metal based catalysts [9,10]. The reduction of UO_2^{2+} ions to U^{4+} ions has been studied by electrocatalytic [11], photocatalytic [7,12], sonolysis [13], and chemical reduction methods [14,15]. For the remediation objectives, an interesting approach has been reported by Sheng et al. which involves adsorption and reduction of UO_2^{2+} to U^{4+}, formation of UO_2 particles and finally retention of the particles using hosts such as haematite, titanate nanotubes, and nanoscale zero-valent iron immobilized on diatomite or Na−Bentonite [16–19].

Formic acid has been used for the catalyzed reduction of $Cr_2O_7^{2-}/CrO_4^{2-}$ anions to Cr^{3+} ions [20–23], destruction of nitrate

---

ions in the aqueous discharges [24–26], and nitrite reduction in water [27]. The major issues for using Pd nanoparticles (NPs) as a heterogeneous catalyst are their agglomeration, chemical corrosion, surface inactivation, product contamination and recyclability. To address these problems, the noble metal nanocatalysts have been immobilized in a variety of hosts such as inorganic particles (Al_2O_3, SiO_2, TiO_2, Fe_3O_4) [27–30], carbon nanomaterials (carbon nanotubes, graphene oxide, carbon spheres) [31–33], resin beads [34,35], electrospun fibers mats [36,37], hydrogels [38], poly(HIPE) [39], and membranes [40–43]. The Pd NPs formed in the films of poly(vinyl alcohol) and cellulose acetate have been have been used as the "dip catalysts" for the organic reactions [44,45]. The hallmarks of supported Pd NPs not only include chemical and physical stabilities but also simplicity of fabrication, easy retrieval, recyclability and amenability for a scale up. The porous supports like membranes, poly(HIPE) and electrospun fibers mat provide high accessibility to the heterogeneous nanocatalysts that enhances the catalytic activity [17,39]. The eggshell membrane, having three dimensional fibrous structures, is reported to hold precursor metal ions, reduce them, and protect the metal nanoparticles without affecting their catalytic activity [46,47]. An asymmetric N-methyl-*D*-glucamine grafted membrane has been developed that reduces a variety of precursor ions such as Ag^+, Pd^{2+}, Rh^{3+}, Ru^{3+} and $AuCl_4^-$ ions and stabilizes thus formed NPs in the membrane [48].

To mimic eggshell membrane with a better mechanical properties and highly microporous architecture, the reducing moiety hydrazine has been attached covalently in pores of the microporous host poly(propylene) membrane by first grafting glycidyl methacrylate (GMA) in pores of the membrane by *in situ* UV-initiator induced polymerization process, and reacting the GMA-grafted membrane subsequently with hydrazine. The Pd NPs have been formed in these hydrazine grafted membranes by equilibrating them in solutions containing Pd^{2+} precursor ions for a fixed period of time. For comparison, the cation-exchange membrane has been prepared by the UV-initiator induced polymerization of 2-acrylamido-2-methyl-1-propane sulfonic acid monomer along with cross-linker in the same poly(propylene) microporous host membrane. The Pd NPs in the cation-exchange membrane have been formed by loading Pd^{2+} ions by ion-exchange in the membrane, and subsequent *in situ* reduction with aqueous hydrazine solution. These Pd NPs embedded membranes have been characterized appropriately, and then examined for the representative UO_2^{2+} ions reduction with formic acid under different conditions including high intensity ultrasonication. The kinetics of UO_2^{2+} ions reductions under different experimental conditions have been analyzed in terms of pseudo-first-order, pseudo-second-order, and diffusion controlled model equations.

2. Experimental

2.1. Reagents and apparatus

The poly(propylene) (PP) host membranes having 0.1 μm pore-sizes, thickness 50 μm and nominal porosity 78% were obtained from Sterlitech corporation. Hydrazine hydrate (99%), methanol and HNO_3 (69–70%) were procured from s.d. Fine Chemicals, Mumbai. Glycidyl methacrylate (GMA), 2-acrylamido-2-methyl-1-propane sulfonic acid (AMPS), spacer (3-acryloxypropyl)trimethoxysilane (APTMS), α,α′-dimethoxy-α-phenylacetophenone (DMPA), and ethylene glycol dimethacrylate (EGDM) were obtained from Sigma-Aldrich (Steinheim, Switzerland). Acetone, palladium chloride and formic acid (98–100%) were procured from Sisco Research laboratories Pvt. Ltd, India, Research-lab Fine Chem. Industries, India, and BDH-
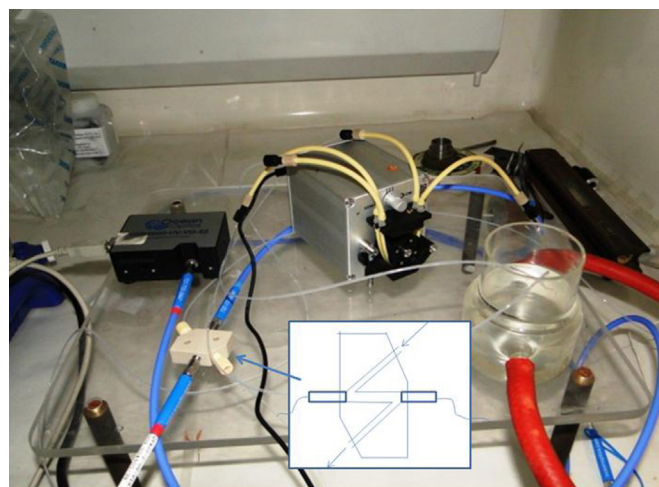

Fig. 1. Setup of Z-flow cell spectrophotometry used for on-line monitoring of UV–vis absorption spectra during reduction of UO_2^{2+} to U^{4+} ions.

Chemicals Ltd, Poole England, respectively. All the reagents used in the present work were A.R. Grade.

The UV-initiator induced grafting of monomers in the polymer membranes were carried out in a Heber Scientific, Chennai, India make UV multilamps photoreactor having 8 lamps (λ_{max} = 365 nm, 8 W, Sankyo Denki, Japan) fitted in a circular geometry. Ultrasonic laboratory processor (model SONAPROS PR-500MP, SS Horn having 12 mm dia., 20 ± 3 KHz) was procured from Oscar Ultrasonics Pvt. Ltd., India. UV–vis spectrophotometer model V 53 from JASCO (Tokyo, Japan) was used to record successive UV–vis absorption spectra during reduction of UO_2^{2+} to U^{4+} ions. On-line monitoring of UO_2^{2+} ions reduction was carried out by pumping reaction solution to 10 mm path length Z-cell (FIA-1000-Z, Ocean Optics) using peristaltic pump. The Z cell was connected to light source (AvaLight-DH-S-BAL) and spectrometer (USB4000-UV–VIS–ES, Ocean optics) at opposite sides with 400 μm optical fibers. The photograph of this setup is shown in Fig. 1.

2.2. Formation of Pd NPs embedded neutral membrane

The precursor membranes were prepared by UV-initiator (DMPA) induced *in situ* polymerization of monomer (GMA) along with cross-linker (EGDM) in pores of the microporous PP host membranes. The polymerizing solution for pore-filling in the PP membranes was prepared by dissolving 1.5 g of GMA in 2 mL of DMF solvent, and adding 5 mol% of cross-linker (EGDM) and 2 wt% of UV-initiator (DMPA). The polymerizing solution thus formed was sonicated for 15 min for homogenization before pore-filling. The membrane samples having 5×5 cm^2 area were soaked first in methanol for 3 h and then immersed in the polymerizing solutions overnight. After pore-filling, solution adhering to surfaces of the host membranes was removed gently with Teflon roller. The polymerizing solution filled membranes were sandwiched between two Garware polyester sheets and irradiated with 365 nm light in a photoreactor for a period of 30 min. After polymerization, the membrane samples were first washed thoroughly with DMF/ethanol and then with water to remove un-polymerized components from the membranes. The membrane samples were washed till constant weights were obtained.

The poly(GMA)-grafted membranes were reacted with hydrazine hydrate (99%) for 12 h with constant stirring at room temperature. The hydrazine reacted polymer membranes were thoroughly washed with deionized water several times to remove un-reacted hydrazine, and vacuum dried for further use. The attachment of hydrazine with the glycidyl units grafted in the PP

membrane was monitored by nitrogen analysis. These hydrazine attached membranes were equilibrated with the solutions containing 0.01 mol L^{-1} PdCl$_2$ at pH = 3 or 1 for a predetermined time period to form controlled amount of Pd NPs in the membrane.

2.3. Formation of Pd NPs embedded cation-exchange membrane

The cation-exchange membranes were prepared using similar procedure described in our earlier publication [49]. Briefly, the sulfonic acid monomer AMPS and silane based monomer APTMS were taken in 1:1 mol proportion along with 2 wt% UV-Initiator (DMPA) and 5 mol% of cross-linker (EGDM) and were dissolved in DMF solvent to form a polymerizing solution. The silane monomer APTMS was used as filler to minimize dimensional changes and brittleness in the dry state as observed in the cation-exchange membrane prepared without using APTMS. The polymerizing solution was filled in the PP membrane in a similar procedure described for GMA grafting, and exposed to 365 nm UV light for 30 min, Ungrafted components were removed by washing with DMF and water. After grafting, the membrane was conditioned in 0.1 mol L^{-1} NaCl solution for 24 h, and then equilibrated with 0.01 mol L^{-1} PdCl$_2$ solution overnight to load Pd^{2+} ions by the ion-exchange mechanism. The Pd^{2+} ions loaded membrane samples were immersed in 10% v/v hydrazine aqueous solution to reduce Pd^{2+} ions held at the ion-exchange sites to Pd^0.

2.4. Characterizations of membranes

The amounts of Pd^0 loaded were determined by leaching out Pd^0 in aqua-regia solution for 12 h at room temp. from the membranes sample having known dimension (2 × 1 cm^2) and weight. The leach liquor was evaporated to dryness under IR heating and redissolved in 10 mL of 0.1 mol L^{-1} HNO$_3$. The complete leaching of Pd^0 was confirmed by EDXRF analyses of the membrane sample before and after leaching. These solutions were subjected to ICP-AES analyses for the determination of conc. of Pd, which was used to calculate the amount of Pd content loaded in the membrane sample. The ICP-AES analyses were done using high resolution simultaneous atomic emission spectrometer (Spectro Arcos, Germany) with ICP and DC arc as the excitation sources and a charge-coupled device (CCD) as the detector. It had a continuous wavelength coverage of 130–800 nm with resolution of 0.01 nm from 130 to 450 nm and 0.02 nm from 450 to 800 nm. The instrumental specifications and experimental details are described elsewhere [50].

The void volumes (vol.%) of the pristine membrane, hydrazine grafted membrane and Pd NPs embedded membrane samples were measured by using wetting liquid "Porefil" liquid (γ = 0.016 N m^{-1}) supplied by Benelux Scientific, Belgium using following eq.

$$Void\ Volume = \frac{(w_l - w_d)}{\rho_l V_m} \times 100 \qquad (1)$$

Where w_l, w_d, ρ_l and V_m were weight of Porefil liquid wetted membrane sample, weight of dry membrane, density of Porefil liquid, and volume of the membrane sample, respectively. The membrane sample having the known dimensions (V_m) and weight (w_d) was immersed in Porefil liquid for 4–5 h, removed liquid clinging on the surface gently, and weighed to obtain the weight of wetted membrane (w_l). The dimensions of the membrane did not change after wetting in Porefil liquid. The pore-size distributions were measured by capillary flow porometry (CFP) using Porefil liquid as described elsewhere [51]. Capillary flow porometry (CFP) measures the most constricted part of through pores based on the measurement of the pressure necessary to blow gas through a liquid-filled porous membrane which can be correlated to the pore diameter using Washburn equation [51]. The CFP measurements were carried out using the porometer model POROLUX^{TM} 1000 (Benelux Scientific,

Belgium), and data acquisition and analysis was carried out using LabView software supplied by manufacturer. The Porefil liquid wetted membrane sample was mounted in a 25 mm diameter sample holder and a wet run was performed that was followed by dry run (sample without wetting liquid) for obtaining flow rate curves as a function of applied pressure.

The FE-SEM imaging of the pristine and the Pd NPs embedded grafted membranes were done using Model No. JSM-7600F at SAIF, IIT-B, Mumbai, India. The samples were coated with gold prior to microscopy to make them conducting. The elemental mappings of Pd across the cross-section and surface were carried out by energy dispersive spectroscopy (EDS). The acidity/basicity of the membrane samples was measured by HCl-NaOH titrations.

2.5. Reduction of UO$_2$$^{2+}$ ions

The reduction of UO$_2$$^{2+}$ ions was carried out in a double jacketed glass vessel kept at constant temperature using thermostat bath. The reaction solution was prepared by mixing equal volumes (8 mL) of 0.1 mol L^{-1} UO$_2$(NO$_3$)$_2$ solution at pH = 2 and 1 mol L^{-1} formic acid. This solution was poured in the reaction vessel kept at a fixed temp. (25, 40, 50 or 60 °C). The Pd-loaded PP membrane having fixed dimensions (1 × 2 cm^2 membrane) or known weights were immersed in the stirred (300 rpm) reaction solution attained with desirable temp. The immersion time was taken as start time and no UO$_2$$^{2+}$ ions reductions was observed without catalyst and with catalyst at room temp. as can be seen from UV–vis spectra which were showing no characteristic absorption peaks of U^{4+} ions, see Fig. 2.

The progress of reduction of UO$_2$$^{2+}$ ions was monitored by taking 1 mL aliquot from the reaction solution at a fixed time interval, and UV–vis spectra of these samples were recorded after diluting this to 3 mL by adding pH = 2 solution. Similar experiment was done with high intensity ultrasonication by immersing SS horn in the reaction solution. The reaction solution temp. at 150 W power sonication was increased to 60 °C. Therefore, the Pd NPs embedded PP membrane sample was introduced after allowing reacting solution to attain constant 60 °C temp. For on-line monitoring, reaction solution was circulated to Z flow cell with peristaltic pump with constant speed (2 mL min^{-1}) and successive UV–vis absorption spectra were recorded at 5 min time intervals. For kinetic experiments, the most intense peak of U^{4+} ion at 665 nm was calibrated by measuring the U^{4+} ions concentration by electroanalysis. To prevent back oxidation of U^{4+} ions to UO$_2$$^{2+}$ ions during a long storage, the solution was kept in a freezer and UV–vis spectra was monitored again to ensure the extent of oxidation of U^{4+} ions.

The quantification of formation of U^{4+} ions was carried out by controlled potential coulometric method. CHI 760D electrochemical work station was used for carrying out coulometry. The working electrode was hollow cylindrical platinum wire gauze of 0.07 m height and 0.032 m diameter. The counter electrode was a thin platinum wire. The reported potentials were with respect to the saturated Ag/AgCl. All the experiments were carried out at room temperature. The concentration of U^{4+} ions was determined employing controlled potential coulometry. For activation of platinum electrode prior to the experiments, the electrode was submerged in 1 mol L^{-1} H$_2$SO$_4$ and was anodized at 1.4 V for 15 min. This was immediately followed by cathodization in the same electrolyte at 0.150 V vs. Ag/AgCl until the current reached the background level of 25 μA. The aqueous samples (25 mL of solution of U^{4+} ions in formic acid) were subjected to the oxidation of U^{4+} to UO$_2$$^{2+}$ ions at potential of +1.4 V. Electrolysis was terminated at the background current level. The total charge obtained for the oxidation was noted and the amount of U^{4+} oxidized to UO$_2$$^{2+}$ ions was calculated using Faraday's first law of electrolysis.

Fig. 3. Comparison of pore-size distributions obtained by capillary flow porometry in the pristine poly(propylene) membrane, hydrazine-grafted poly(propylene) membrane, and Pd NPs embedded membrane samples.
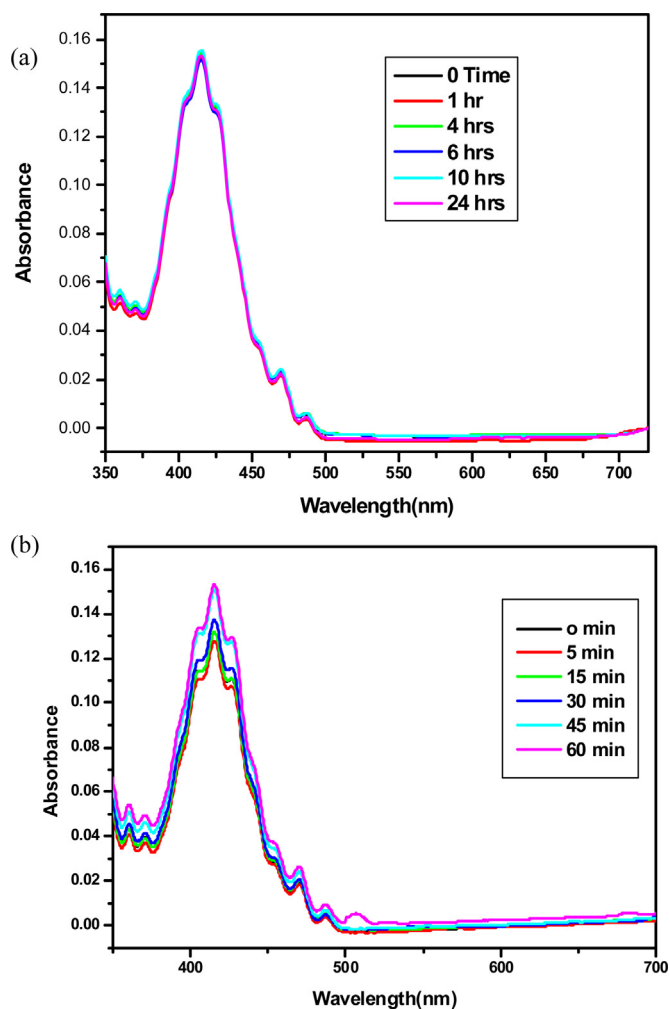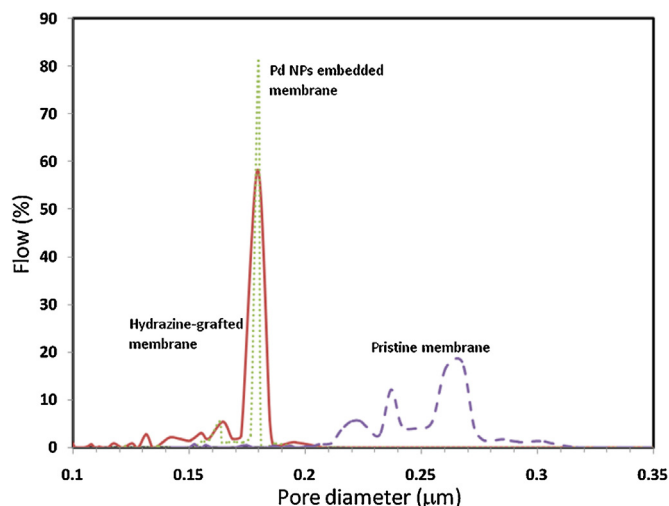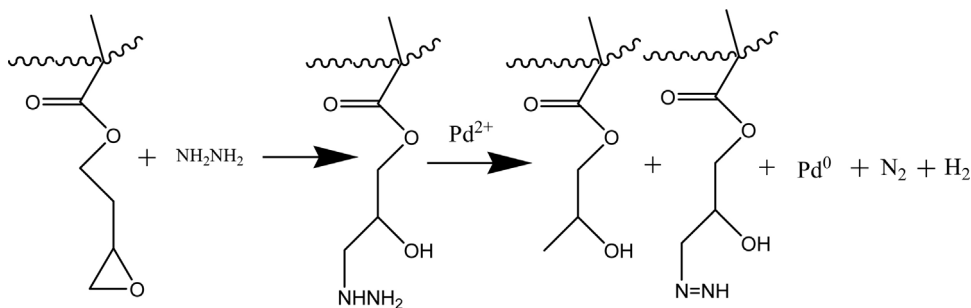

Fig. 2. Successive UV–vis spectra showing reduction of UO_2^{2+} to U^{4+} ions using formic acid: (a) in the presence of Pd NPs embedded hydrazine-grafted PP membrane at room temp., and (b) in the presence of hydrazine-grafted membrane without Pd NPs at 50 °C as a function of time.

3. Results and discussion

3.1. Characterizations of Pd NPs embedded membranes

The two types of the membranes developed in the present work were the self-reducing membrane and cation-exchange membrane. This class of pore-filled membranes has two components *i.e.* microporous host membrane to provide support and the cross-linked microgels for the formation and holding Pd NPs in pores. In general, these membranes are prepared by polymerizing solution containing monomers and cross-linker filled in pores of the host membrane. The polymers formed by monomers did not have mechanical properties, but had required functional groups for forming Pd NPs. For making the self-reducing membrane, poly(GMA) was anchored in pores of the microporous membrane. The average mass-gain (grafting yields) obtained from the increase in weight of the pore-filled membrane with respect to pristine membrane was found to be 85 ± 5 (n = 3, where n is no. of exp.) wt%. In pores of the PP membrane, the grafting occurred through hydrogen abstraction from base poly(propylene) chains, and also cross-linked homo-polymer poly(GMA) chains interpenetrating network structure was formed in pores of the membrane. The hydrazine units were attached covalently via glycidyl units in pores of the poly(GMA) anchored membrane. The Pd NPs were formed by

just dipping the hydrazine-grafted membrane in a $PdCl_2$ solution having fixed pH. The possible reactions during different chemical treatments involved in the formation of Pd NPs in the membrane are shown in Scheme 1.

The saturation loading of Pd^0 in the hydrazine grafted membrane was found to be 124 ± 1 mg g^{-1} (n = 3) after 15 h equilibration in solution having 0.01 mol L^{-1} $PdCl_2$ at pH = 3. The nitrogen contents of the hydrazine grafted PP based membrane samples were found to be 4.2 and 2.1 wt% before and after saturation loading of Pd^0 content, respectively. This seems to suggest that all hydrazine units were not utilized for the reduction of Pd^{2+} ions. The basicity of the hydrazine-grafted membrane was found to 1.55 ± 0.05 meq g^{-1} which was reduced to 0.5 ± 1 meq g^{-1} after the formation of Pd NPs. The statistical uncertainty quoted is for duplicate experiments (n = 2). This indicated that the residual hydrazine was left after the formation of Pd NPs that could facilitate the reduction of UO_2^{2+} ions as observed in the case of formic acid decomposition [30], which was used as reductant. The importance of residual hydrazine was observed from the fact that the Pd NPs loaded membrane having negligible basicity (0.0005 meq g^{-1}) did not show significant catalytic activity in the reduction of UO_2^{2+} ions with formic acid at 50 °C. This membrane was formed by equilibrating the hydrazine-grafted membrane in the solution having 0.01 mol L^{-1} $PdCl_2$ at pH = 1 for 15 h that lead to quantitative reduction of Pd^{2+} ions and consumed nearly all hydrazine groups in the membrane. To explore a possibility of increasing saturation Pd^0 loading capacity of the membrane, the grafting yield of GMA was increased by increasing its conc. in the polymerizing solution. This resulted in an increase in the mass-gain from 85 ± 5 wt% to 155 ± 5 wt%, and Pd saturation loading capacity from 124 ± 1 mg g^{-1} to 200 ± 5 mg g^{-1}. However, the Pd NPs loaded membrane with 85 wt% mass-gain was used for further studies as the porosity would be reduced and pores may be blocked in the membrane sample having higher mass-gain.

The void volume of the hydrazine-grafted membrane sample was found to 35 v/v% which was significantly lower than the pristine membrane (86 v/v%). However, there was no significant change in the void volume of membrane sample after the formation of Pd NPs (34 v/v%). This seems to suggest that the Pd NPs loaded hydrazine-grafted membrane had porosity to an extent of 34 v/v%. To study the change in distribution of through-pore sizes, the pristine, hydrazine-grafted, and Pd NPs embedded membrane samples were subjected to capillary flow porometry. Thus obtained pore-size distributions are shown in Fig. 3 in which flow (%) given in

Scheme 1. Chemical modifications involved in the formation of Pd NPs in the neutral PP membrane.
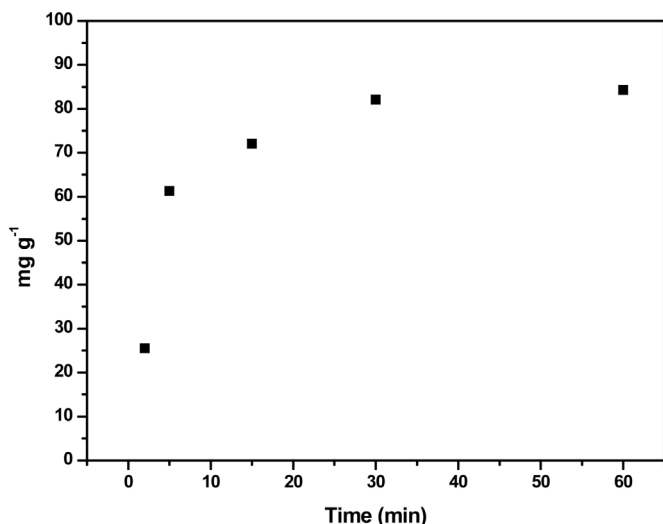

Fig. 4. Variation of Pd^0 content in the hydrazine-grafted membrane sample as a function of equilibration times in the well-stirred aqueous solution containing $0.01 \, mol \, L^{-1}$ PdCl$_2$ at pH = 3.

y-axis is a measure of number density as described elsewhere [51]. The important observations of the pore-size distributions obtained from capillary flow porometry are: (i) Pd NPs membrane had through pores, (ii) pore-size reduced after hydrazine grafting to $0.18 \, \mu m$ but did not further reduce after formation of Pd NPs, and (iii) and pore-size distribution became narrower after hydrazine grafting which was further improved after formation of Pd NPs. This seems to suggest that there was a change in the physical structure of hydrazine-grafted membrane during the course of formation of Pd NPs.

The Pd^0 content in the membrane could be controlled by its equilibration time in the solution containing Pd^{2+} ions. As can be seen in Fig. 4, the Pd^0 loading was fast within 30 min equilibration ($82 \, mg \, g^{-1}$), and became very slow thereafter. The saturation loading of Pd^0 in the hydrazine grafted membrane was $124 \pm 1 \, mg \, g^{-1}$ under similar conditions. It is evident from the curves of variation of Pd^0 content in the membrane sample as a function of equilibration time that the desirable amount of Pd^0 could be loaded only up to the saturation loading. The expected amount of saturation loading of Pd^0 content in the hydrazine grafted membrane was expected to be $152 \, mg \, g^{-1}$ based on 50% reduction of nitrogen content, which was comparable to the experimental saturation loading $124 \pm 1 \, mg \, g^{-1}$. Thus, the most of the Pd^0 content (80%) was retained in the membrane in the form of Pd NPs.

In the case of cation-exchange membrane, the mass-gain after grafting was found to $170 \pm 5 \, wt\%$ in the same host PP microporous membrane. The ion-exchange capacity of this membrane (acidity) was found to be $1.6 \pm 0.2 \, meq \, g^{-1}$. The formation of Pd NPs in the cation-exchange membrane involved two steps process as

shown in Scheme 2. First, the precursor Pd^{2+} ions were loaded in the membrane by the ion-exchange mechanism. Subsequently, the Pd^{2+}-loaded membrane was subjected to reduction with hydrazine.
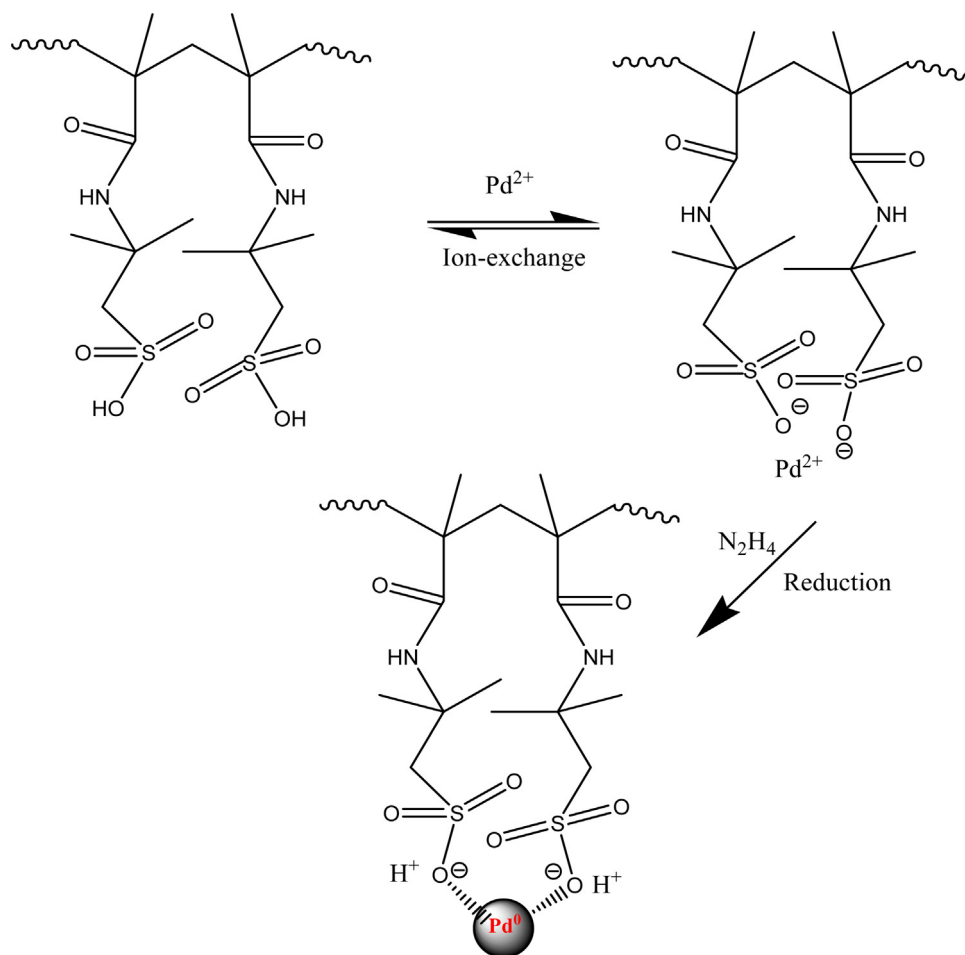
The saturation Pd^0 loading in the cation-exchange membrane sample was $13 \pm 2 \, mg \, g^{-1}$, which was considerably lower than that in the hydrazine-grafted membrane sample. The Pd^0 loading capacity was 6–7 times lower than the expected saturation loading. This may be due to either inefficient reduction of Pd^{2+} ions in the acidic environment or slow reduction process leading to a substantial loss of Pd^0 seeds before locking as NPs in the membrane [52]. In hydrazine grafted membrane, the reduction of Pd^{2+} would be fast and dependent only on the diffusion of Pd^{2+} ions in the pores of membrane leading to a high Pd NPs content. However, the Pd^0 loading could be improved in the cation-exchange membrane by repeating cycle of loading of Pd^{2+} ions and subsequent reduction with hydrazine to form Pd^0 and regenerating ion-exchange sites as shown in Scheme 2.

The Pd NPs embedded membranes developed in the present work were analyzed by FE-SEM imaging and elemental mappings of the surfaces as well as the cross-sections of the samples. The N and Pd elemental EDS mappings across the thickness of the hydrazine grafted membrane sample given in Fig. 5(a & b) seems to suggest a uniform hydrazine grafting and Pd NPs distribution, respectively, throughout the membrane matrix. A comparison of the FE-SEM images of Pd NPs loaded hydrazine grafted PP membrane with that of the pristine PP membrane indicated high porosity of the Pd NPs embedded neutral membrane as expected from the experimentally measured void volume, see Fig. 5(c–f). The high porosity is important for the Pd NPs to be accessible to the reactants for stronger catalytic activity. It is seen from Fig. 5(c & d) that $17 \pm 4 \, nm$ size Pd NPs were formed on the surfaces of PP membrane after saturation loading. However, the size of Pd NPs were much smaller (<5 nm) at the interior matrix and could be distinguished from the polymer matrix only by EDS mappings, see Fig. 5(a & b). The sizes of Pd NPs were much smaller than pore size ≈180 nm that ensured possibility for the reactants and catalyst to come in a contact.

The physical structure of the membrane and distribution of Pd NPs in the cation-exchange membrane were also studied using FE-SEM/EDS. It is seen from the FE-SEM images of surface and cross-section of the PP based cation-exchange membrane shown in Fig. 6 that this membrane had a porous physical structure similar to hydrazine grafted PP membrane and Pd NPs were uniformly distributed throughout the matrix as indicated by the Pd elemental mapping. Thus, Pd NPs in both the membrane could be compared for their catalytic activity.

3.2. Comparison of catalytic activities of Pd NPs embedded membranes

Pd NPs catalyzed UO$_2$$^{2+}$ ions reduction with formic acid. Formic acid is a two electron transfer reductant with a potential $-0.199 \, V$ for HCOOH/CO$_2$, 2H$^+$ couple. Although redox potential of

Scheme 2. Representative steps involved in the formation of Pd NPs in cation-exchange membrane.

$UO_2^{2+} + 2e^- \rightarrow U^{4+}$ couple is 0.41 V vs. standard hydrogen electrode [13], the UO_2^{2+} ions reduction does not occur in the absence of Pd catalyst or with catalyst at room temp. as shown in Fig. 2. This seems to suggest a high activation barrier in the UO_2^{2+} ions reduction. In additions to this, the Pd NPs are known to catalyze decomposition of formic acid [34,53], that would not only compete with UO_2^{2+} ions reduction but also deactivate the Pd NPs by hydrogen and carbon monoxide sorption. The different competing reactions are shown below:

$$HCOOH \rightarrow H_2 + CO_2 \quad (2)$$

$$HCOOH \rightarrow H_2O + CO \quad (3)$$

$$HCOOH \rightarrow CO_2 + 2H^+ + 2e^- \quad (4)$$

To understand the effect of temperature on the Pd NP catalyze reduction of UO_2^{2+} ions, the conc. of UO_2^{2+} ions as a function of reduction time with formic acid was analyzed by pseudo-first-order kinetic equation that is normally applicable in the presence of excess of reducing agent [48]. A detailed analysis is given in later part of the paper. It is seen from Fig. 7 that the variations of ln $[U(VI)]_t/[U(VI)]_0$ as a function of reduction time with formic acid in the presence of Pd embedded PP membrane at different temperature is reasonably linear as expected from first-order kinetic equation given below and could be used for a qualitative comparison, though correlation coefficients ($R^2 = \approx 0.98$) indicated not the best fits.

$$\ln\left(\frac{[U(VI)]_t}{[U(VI)]_0}\right) = -kt \quad (5)$$

Where $[U(VI)]_t$ and $[U(VI)]_0$ represent conc. of UO_2^{2+} ions at time t and initial, respectively, t is reduction time, and k is apparent first-order reduction rate constant. As k is dependent on the amount of Pd catalyst, the values of k were normalized with the amount of Pd^0 to obtain catalytic activity ($s^{-1} g^{-1}$) for studying the effect of variables involved in the reduction of UO_2^{2+} ions with formic acid.

The values of catalytic activities of the Pd NPs embedded hydrazine grafted PP membranes at 40, 50 and 60 °C temperatures were found to be 0.11, 0.39 and 0.46 $s^{-1} g^{-1}$, respectively. This seems to suggest that there was significant jump of the catalytic activity at 50 °C and increased slowly thereafter. There was a critical minimum quantity of Pd NPs catalyst (0.20 mg) needed for the reduction reaction to take place at 50 °C. It is seen from Fig. 8 that the catalytic activity of Pd NPs in UO_2^{2+} reduction increased with increase in amount of Pd NPs to attain optimum value 0.39 $s^{-1} g^{-1}$, but decreased subsequently on further increase of the Pd NPs content. This could be indicative of the onset of formic acid decomposition as shown in Eqs. (2) & (3) in the presence of high amount of Pd NPs catalyst. Thus, an optimum amount of Pd NPs is required for the efficient reduction. The catalytic activity of Pd/C (5 wt%) was found to be 0.13 $s^{-1} g^{-1}$ under similar conditions, which was significantly lower than the 0.39 $s^{-1} g^{-1}$ obtained using the Pd NPs embedded hydrazine grafted membrane.

Contrary to Pd NPs in the hydrazine-grafted membrane host, the Pd NPs embedded in cation-exchange membrane did not show any catalytic activity in the reduction of the UO_2^{2+} ions with formic acid, Fig. 9a. To ensure that the UO_2^{2+} ions reduction is not affected by the conc. of Pd NPs in the cation-exchange membrane, the Pd
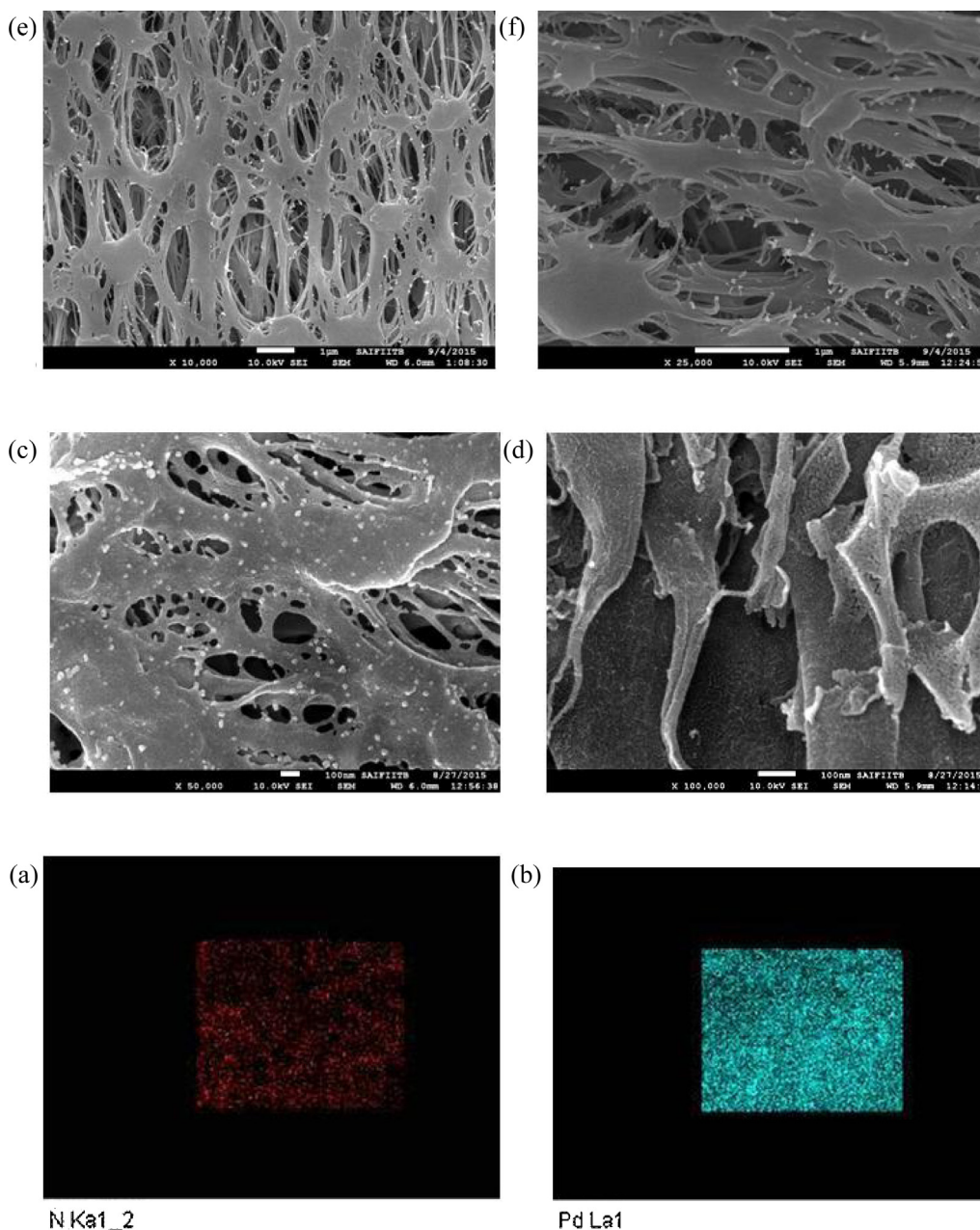
Fig. 5. The representative EDS elemental mappings of nitrogen (a) and Pd (b) at cross-sections ($4 \times 4 \mu$m) of the same Pd NPs embedded hydrazine-grafted membrane, and FE-SEM images of (c) surfaces of Pd NPs embedded hydrazine grafted membrane, (d) cross-section of Pd NPs embedded hydrazine-grafted membrane, (e) surface of pristine PP membrane, and (f) cross-section of pristine PP membrane.

content was boosted to approximately four times by repeating a cycle of Pd^{2+} ions loading and reduction in the cation-exchange matrix four times. Even using this Pd NPs loaded membrane, the extent of UO_2^{2+} reduction was not very significant (less than 5% in 60 min) as shown in Fig. 9b.

It appears that the absence of catalytic activity of Pd NPs in the cation-exchange matrix could be related to binding of UO_2^{2+} ions with the fixed negative charge sites ($-SO_3^-$) in cation-exchange matrix which would hinder UO_2^{2+} ions interactions with Pd NPs required for the reduction with formic acid as shown in Scheme 3. It is also important to note from the UO_2^{2+} ions reduction carried out in the presence of Pd NPs embedded hydrazine-grafted membrane that basic local environment (caused by residual hydrazine) is also required for the efficient reduction UO_2^{2+} ions with formic acid.

3.3. Quantification of UO_2^{2+} ions reduction with formic acid

The conversion of UO_2^{2+} ions to U^{4+} ions by formic acid in the presence of Pd NPs embedded hydrazine grafted PP membrane at 50 °C were monitored by online spectrophotometry using a setup shown in Fig. 1. It is obvious from Fig. 10 that the absorbance peaks of U^{4+} ions increased continuously as a function of reduction time and saturated at 70 min. It was observed that >99% UO_2^{2+} ions were reduced to U^{4+} ions during 70 min reduction time under the conditions stated in the experimental section.

As can be seen from a comparison of absorption peaks of U^{4+} ions given in Table 1, the absorption peaks monitored in the reaction solution were red-shifted with respect to that expected in a solution having no complexing ions [54].This could be attributed to unused formate ions which formed complex with U^{4+} ions leading to red shifting of the absorption peaks corresponding to f–f tran-
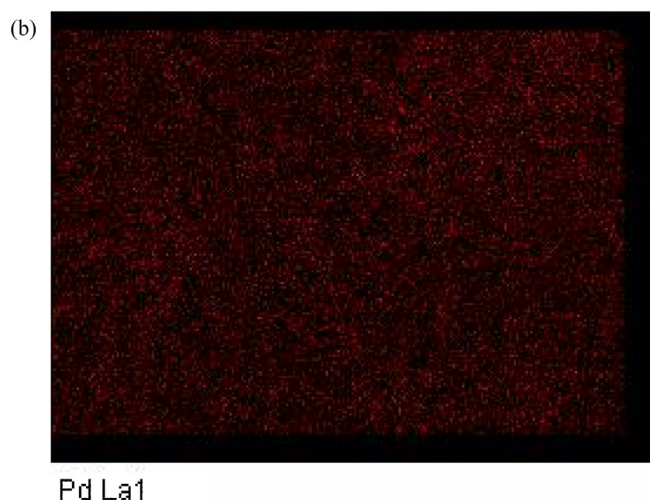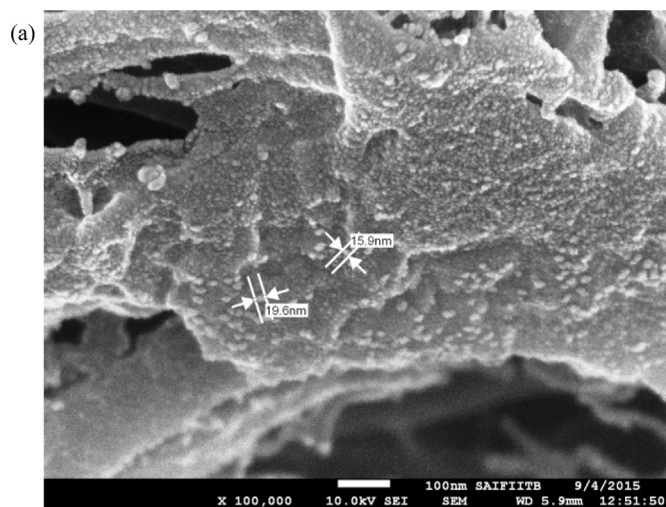
Fig. 6. Representative FE-SEM images of surface (a) of PP membrane based cation-exchange membrane, and elemental mapping of Pd (b) at cross-section ($5 \times 6\,\mu$m) of the same membrane.
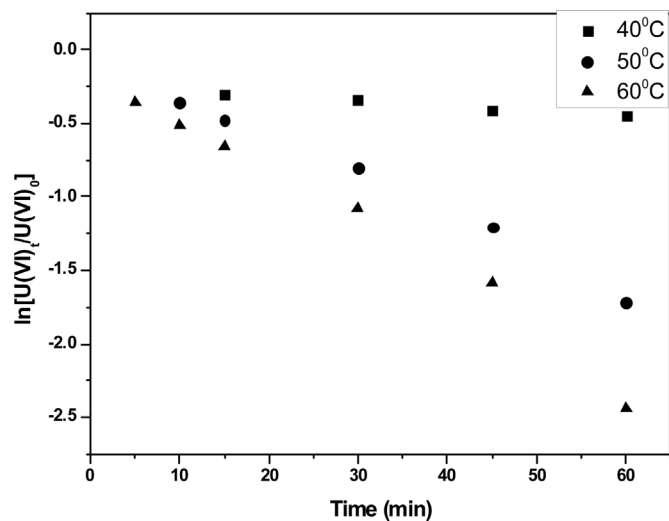

Fig. 7. Variation of logarithm of $[U(VI)]_t/[U(VI)]_o$ as a function of reduction time with formic acid in the presence of Pd embedded PP membrane at 40, 50, 60 °C temp. $[U(VI)]_t$ and $[U(VI)]_o$ represent conc. of UO_2^{2+} ions at time t and initial, respectively.
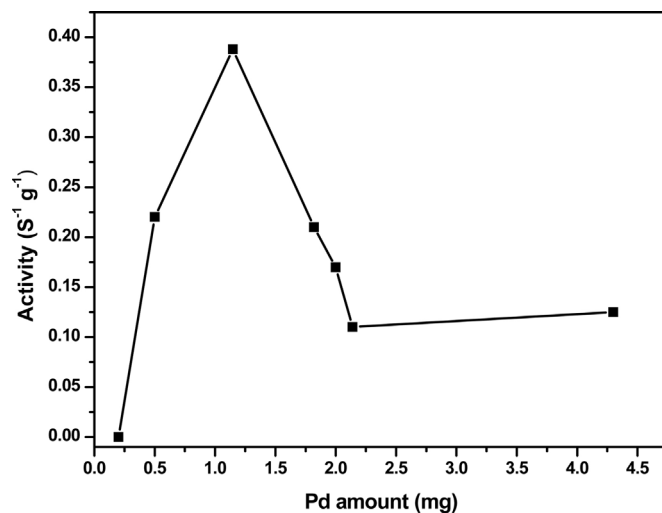

Fig. 8. Variation of catalytic activity of the Pd NPs embedded in hydrazine-grafted membrane as a function of Pd^0 content in the reduction of UO_2^{2+} ions by formic acid to U^{4+} ions at 50 °C.
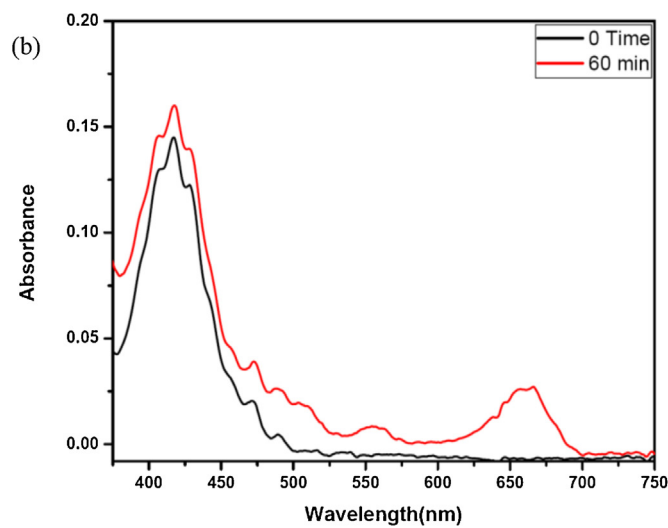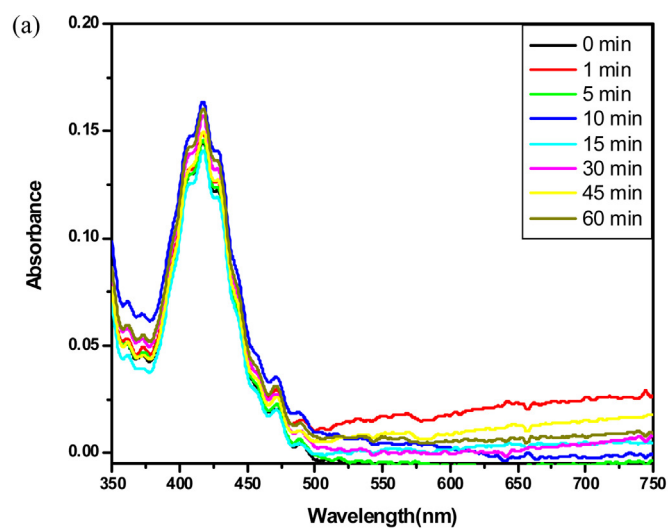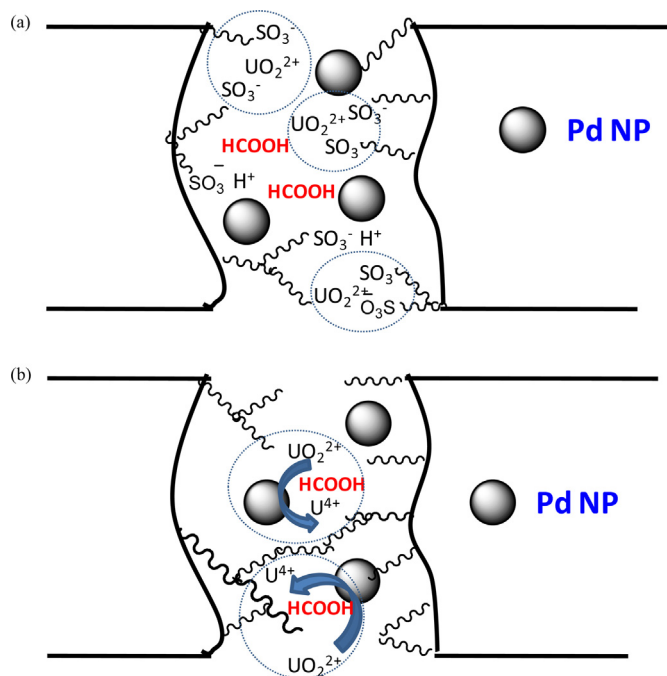

Fig. 9. UV–vis spectra showing no reduction of U(VI) with formic acid in the presence of Pd NPs immobilized in the cation-exchange membrane at 50 °C. Figs. a & b present the experiments carried out using the cation-exchange membrane loaded with Pd NPs in one cycle and four cycles, respectively.

Scheme 3. Preferential UO_2^{2+} ions interactions with sulfonic acid groups in a pore of Pd NPs embedded cation-exchange membrane (a), and with Pd NPs in hydrazine-grafted membrane (b).
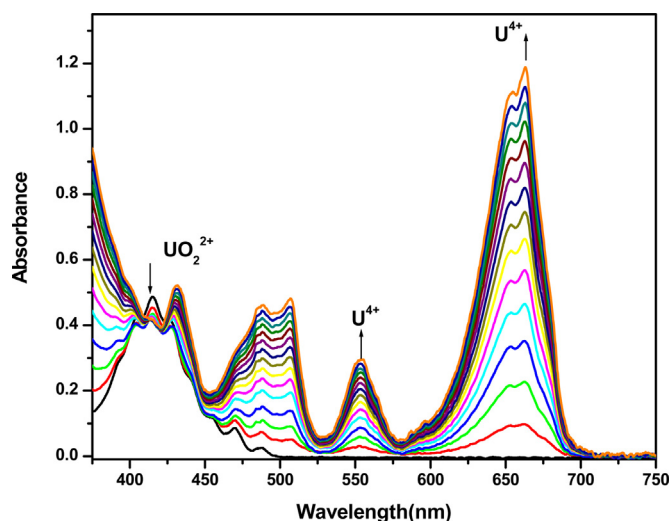

Fig. 10. The successive UV–vis spectra obtained online after every 5 min intervals during 70 min reduction of UO_2^{2+} ions with formic acid in the presence of Pd NPs embedded hydrazine-grafted PP membrane at 50 °C.

Table 1
Comparison of absorption energy levels for U^{4+} ion in solution [Ref. [49]] and observed in the present work due to its complex formation with formate.

Transition	Expected λ (nm)	Observed λ (nm)
$^3H_4$-$^1G_4$	644	665
$^3H_4$-$^1D_2$	631	654.3
$^3H_4$-$^3P_1$	546	555
$^3H_4$-$^1I_6$	471	489.4
$^3H_4$-$^3P_2$	427	434.6

sitions in the UV–vis spectrum. The formation of formate complex would provide stability of U^{4+} ions during storage under ambient conditions.
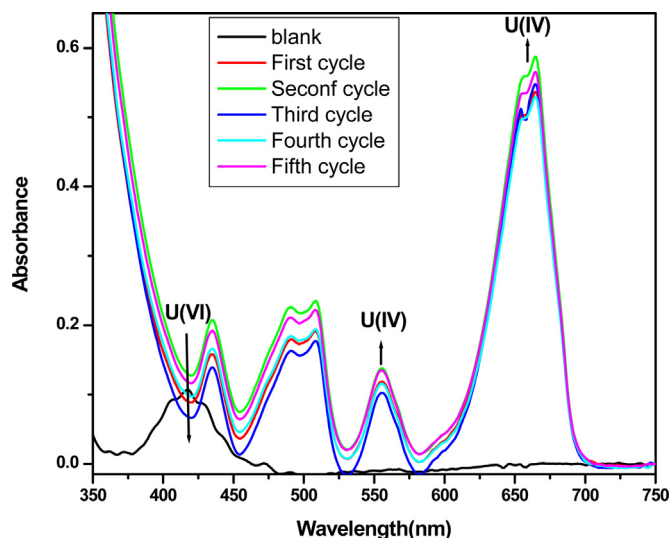

Fig. 11. UV–vis spectra showing the absorbance peaks corresponding to U^{4+} ions after 1 h successive cycles of the reduction of UO_2^{2+} ions with formic acid in the presence of Pd embedded PP membrane.

The oxidation of U^{4+} ions occurs readily at ambient conditions in solution. Therefore, the storage of solution is difficult and U^{4+} ions have to be precipitated as UO_2 by adjusting pH to 9 with NaOH. In the present work, the reaction solution was stored at −4 °C for a month. The UV–vis spectra of freeze-stored solution indicated that U^{4+} ions did not oxidize back to UO_2^{2+} ions during one month storage. However, the U^{4+} ions were oxidized back completely to UO_2^{2+} ions kept at room temperature (25 °C) for 7 days. The reusability of the Pd NPs embedded PP membrane was tested by repeating cycle of UO_2^{2+} ions reductions at 50 °C under identical conditions for 1 h. UV–vis spectra obtained after the end of each cycle are compared in Fig. 11. It is seen from this comparison that the catalytic activity of the Pd NPs embedded PP membrane did not deteriorate even after five cycles. The Pd NPs embedded in the PP membrane was stored for three months under ambient conditions. The experiments showed that the catalytic activity of this sample did not change significantly after storing for three months.

3.4. Kinetic of reduction

In general, the kinetic of reduction is analyzed by the pseudo-first-order kinetic model represented by Eq. (5). However, it is known that the reaction/sorption kinetics obeys pseudo-first-order kinetics at high initial conc. of solute and pseudo-second-order kinetics at lower initial concentration of reactant/solute [55,56]. Also, the reduction would proceed in the host polymer matrix having interconnecting tortuous pores. This may lead to a diffusion controlled reduction process. To clarify a controlling mechanism operating in the reduction process, the reduction profiles of the UO_2^{2+} ions were analyzed in terms of pseudo-first-order, pseudo-second-order, and inter-particle diffusion kinetics models using linearized Eqs. (5)–(7), respectively [56].

$$\frac{t}{[U(VI)]_t} = \frac{1}{k_2[U(VI)]_e^2} + \frac{t}{[U(VI)]_e} \qquad (6)$$

$$[U(VI)]_t = k_d t^{1/2} \qquad (7)$$

Where $[U(VI)]_t$ and $[U(VI)]_e$ represent concentration of UO_2^{2+} ions at time t and at equilibrium, respectively. k_2 and k_d are the apparent pseudo-second-order rate constant and apparent diffusion rate constant, respectively, and t is the reduction time. The analyses of reduction kinetic using these three kinetic models under identical

Table 2
Analyses of the kinetics of UO_2^{2+} ions reduction with formic acid in the presence of Pd NPs hosted in the hydrazine-grafted PP membrane. The chemical conditions were kept constant and varied either temperature or catalyst amount.

Temp. (Pd amount)	Plot	Correlation coefficient (R^2)	Kinetics of sorption
40 °C	$\ln [(U(VI)]_t/[U(VI)]_0$ vs. t	0.971	Pseudo-first-order
(1.15 mg)	$t/[U(VI)]_t$ vs. t	0.998	Pseudo-second-order
	$[U(VI)]_t$ vs. $t_{1/2}$	0.968	Diffusion controlled
50 °C	$\ln [(U(VI)]_t/[U(VI)]_0$ vs. t	0.988	Pseudo-first-order
(1.15 mg)	$t/[U(VI)]_t$ vs. t	0.869	Pseudo-second-order
	$[U(VI)]_t$ vs. $t_{1/2}$	0.999	Diffusion controlled
60 °C	$\ln [(U(VI)]_t/[U(VI)]_0$ vs. t	0.972	Pseudo-first-order
(1.15 mg)	$t/[U(VI)]_t$ vs. t	0.759	Pseudo-second-order
	$[U(VI)]_t$ vs. $t_{1/2}$	0.999	Diffusion controlled
50 °C	$\ln [(U(VI)]_t/[U(VI)]_0$ vs. t	0.993	Pseudo-first-order
(0.51 mg)	$t/[U(VI)]_t$ vs. t	0.993	Pseudo-second-order
	$[U(VI)]_t$ vs. $t_{1/2}$	0.999	Diffusion controlled
50 °C	$\ln [(U(VI)]_t/[U(VI)]_0$ vs. t	0.991	Pseudo-first-order
(1.82 mg)	$t/[U(VI)]_t$ vs. t	0.948	Pseudo-second-order
	$[U(VI)]_t$ vs. $t_{1/2}$	0.992	Diffusion controlled
50 °C	$\ln [(U(VI)]_t/[U(VI)]_0$ vs. t	0.994	Pseudo-first-order
(4.30 mg)	$t/[U(VI)]_t$ vs. t	0.877	Pseudo-second-order
	$[U(VI)]_t$ vs. $t_{1/2}$	0.977	Diffusion controlled

conditions in the presence of Pd NPs in different hosts are given in Table 2. The reduction of UO_2^{2+} ions with formic acid in the presence of Pd NPs embedded membrane was fast and expected to follow the pseudo-first-order kinetics. Contrary to this, the reduction profile followed a pseudo-second-order kinetics. The switching of UO_2^{2+} ions reduction kinetic to diffusion controlled process was observed depending upon temperature of the reacting solution and amount of Pd NPs loaded in the PP membrane. As can be seen from Table 2, the reduction followed the pseudo-second-order at lower temperature (40 °C) and switched to diffusion controlled kinetic with increase in temperature to 50 °C, which was again switched to pseudo-first-order on increasing the content of Pd NPs from 1.82 mg to 4.30 mg. However, high amount of Pd NPs is not desirable as it would promote decomposition reactions shown in Eqs. (2) & (3).

3.5. Enhancement of kinetics of reduction using sonication

High intensity ultrasound in water produces cavitation, heat and agitation, which are extremely useful in a heterogeneous chemical system by improving mass transfer and reaction kinetics [57,58]. It has been reported that high intensity ultrasound accelerates the reduction of UO_2^{2+} ions with hydrazine catalyzed by Pt and in the presence of 2-propanol as an inhibitor for H_2O_2 formation [59]. Therefore, the effects of high intensity ultrasonication on the UO_2^{2+} ions reduction with formic acid was studied in the presence of Pd NPs embedded hydrazine-grafted membrane. It was interesting to note that the kinetic of reduction at same temperature was switched from the diffusion controlled kinetics to pseudo-first-order kinetics. The catalytic activity of the Pd NPs was enhanced two times during ultrasonication ($0.93 \, s^{-1} \, g^{-1}$ from $0.46 \, s^{-1} \, g^{-1}$) obtained at corresponding 60 °C temp. This substantial increase in the catalytic activity of the Pd NPs by ultrasonication could be due to improved mass transfer of the reactants to membrane matrix which is important in such a heterogeneous system. Thus, the reduction process was no longer controlled by the diffusion process in the host PP matrix.

4. Conclusions

A method was developed to host Pd nanocatalysts in the through-pores hydrazine-grafted synthetic polymer membrane for the UO_2^{2+} ions reduction to U^{4+} ions with formic acid. In the absence of ion-exchange/complexing groups, it was difficult to load high amount of precursor Pd^{2+} ions in the membrane. Therefore, the reducing agent hydrazine itself was grafted in pores of the membrane that facilitated high amount of Pd^0 loading, depending upon hydrazine grafting and reduction solution pH, in the form of NPs in membrane under ambient conditions. The presence of residual hydrazine groups was found to be essential for facilitating the reduction of UO_2^{2+} ions by formic acid. The Pd NPs embedded in the highly porous hydrazine grafted PP membrane exhibited a good catalytic activity in the reduction of UO_2^{2+} ions with formic acid that could be further enhanced using high intensity sonication. It was remarkable that the catalytic activity of this Pd NPs embedded membrane did not deteriorate during successive recycling. The analyses of reduction rate under different experimental conditions indicated that the reductions of UO_2^{2+} with formic acid follow presudo-second-order kinetics but switched to diffusion controlled kinetics on increasing the amount of Pd NPs due to matrix effects. However, the enhancement of the reduction of UO_2^{2+} with formic acid under ultrasonication switched the kinetics from diffusion controlled to pseudo-first-order in the presence of lower amount of Pd NPs due to improved mass transfer of reactants to the host membrane matrix. Thus, the hydrazine-grafted membrane developed in the present work mimics egg-shell membrane in terms of formation and stabilization of Pd NPs. In addition to this, it is robust, efficient, recyclable and having a long shelf-life.

References

[1] V.K. Sharma, R. Zboril, R.S. Varma, Ferrates: greener oxidants with multimodal action in water treatment technologies, Acc. Chem. Res. 48 (2015) 182–191.
[2] M.A. Omole, V.A. Okello, V. Lee, L. Zhou, O.A. Sadik, C. Umbach, B. Sammakia, Catalytic reduction of hexavalent chromium using flexible nanostructured poly(amic acids), ACS Catal. 1 (2011) 139–146.

[3] H. Gu, S.B. Rapole, Y. Huang, D. Cao, Z. Luo, S. Wei, Z. Guo, Synergistic interactions between multi-walled carbon nanotubes and toxic hexavalent chromium, J. Mater. Chem. A 1 (2013) 2011–2021.

[4] R.S. Moakhar, G.K.L. Goh, A. Dolati, M. Ghorbani, Sunlight-driven photoelectrochemical sensor for direct determination of hexavalent chromium based on Au decorated rutile TiO_2 nanorods, Appl. Catal. B: Environ. 201 (2017) 411–418.

[5] F. Liu, J. Yu, G. Tu, L. Qu, J. Xiao, Y. Liu, L. Wang, J. Lei, J. Zhang, Carbon nitride coupled Ti-SBA15 catalyst for visible-light-driven photocatalytic reduction of Cr(VI) and the synergistic oxidation of phenol, Appl. Catal. B: Environ. 201 (2017) 1–11.

[6] T.M. McCleskey, T.M. Foreman, E.E. Hallman, C.J. Burns, N.N. Sauer, Approaching zero discharge in uranium reprocessing: photochemical reduction of uranyl, Environ. Sci. Technol. 35 (2001) 547–551.

[7] H. Hu, J.H. Xin, H. Hu, X. Wang, D. Miao, Y. Liu, Synthesis and stabilization of metal nanocatalysts for reduction reactions – a review, J. Mater. Chem. A 3 (2015) 11157–11182.

[8] K. Liu, Y. Wang, P. Chen, W. Zhong, Q. Liu, M. Li, Y. Wang, W. Wang, Z. Lu, D. Wang, Noncrystalline nickel phosphide decorated poly(vinyl alcohol-co-ethylene) nanofibrous membrane for catalytic hydrogenation of p-nitrophenol, Appl. Catal. B: Environ. 196 (2016) 223–231.

[9] C. Lu, P. Zhang, S. Jiang, X. Wu, S. Song, M. Zhu, Z. Lou, Z. Li, F. Liu, Y. Liu, Y. Wang, Z. Le, Photocatalytic reduction elimination of UO_2^{2+} pollutant under visible light with metal-free sulfur doped g-C_3N_4 photocatalyst, Appl. Catal. B: Environ. 200 (2017) 378–385.

[10] A.R. Fox, S.C. Bart, K. Meyer, C.C. Cummins, Towards uranium catalysts, Nature 455 (2008) 341–349.

[11] M. Nogami, Y. Hirose, T. Arai, Y.-Z. Wei, M. Kumagai, Reduction of U(VI) and some fission products in HNO_3 media by galvanostatic electrolysis, J. Alloys Comp. 451 (2008) 358–360.

[12] V.N. Salomone, J.M. Meichtry, G. Zampieri, M.I. Litter, New insights in the heterogeneous photocatalytic removal of U(VI) in aqueous solution in the presence of 2-propanol, Chem. Eng. J. 261 (2015) 27–35.

[13] T. Toraishi, T. Kimura, M. Arisaka, A remote valency control technique: catalytic reduction of uranium(VI) to uranium(IV) by external ultrasound irradiation, Chem. Commun. 15 (2007) 240–241.

[14] M. Yu Boltoeva, V.P. Shilov, A.V. Anańev, Catalytic reduction of U(VI) with formic acid in acid solutions on palladium catalysts, Radiochemistry 50 (2008) 46–51.

[15] M.S. Tyumentsev, Ya. V. Zubavichus, A.A. Shiryaev, A.V. Anańev, Catalytic reduction of U(VI) in H_2SO_4 solutions with hydrazine and formic acid in the presence of bimetallic platinum–ruthenium catalysts, Radiochemistry 56 (2014) 150–155.

[16] D. Zhao, X. Wang, S. Yang, Z. Guo, G. Sheng, Impact of water quality parameters on the sorption of U(VI) onto hematite, J. Environ. Radioact. 103 (2012) 20–29.

[17] G. Sheng, J. Hu, A. Alsaedi, W. Shammakh, S. Monaquel, F. Ye, H. Li, Y. Huang, A.S. Alshomrani, T. Hayat, B. Ahmad, Interaction of uranium(VI) with titanate nanotubes by macroscopic and spectroscopic investigation, J. Mol. Liquids 212 (2015) 563–568.

[18] G. Sheng, P. Yang, Y. Tang, Q. Hu, H. Li, X. Ren, B. Hu, X. Wang, Y. Huang, New insights into the primary roles of diatomite in the enhanced sequestration of UO_2^{2+} by zerovalent iron nanoparticles: an advanced approach utilizing XPS and EXAFS, Appl. Catal. B: Environ. 193 (2016) 189–197.

[19] G. Sheng, X. Shao, Y. Li, Jianfa Li, H. Dong, W. Cheng, Xing Gao, Y. Huang, Enhanced removal of uranium(VI) by nanoscale zerovalent iron supported on Na-bentonite and an investigation of mechanism, J. Phys. Chem. A 118 (2014) 2952–2958.

[20] M. Yadav, Q. Xu, Catalytic chromium reduction using formic acid and metal nanoparticles immobilized in a metal–organic framework, Chem. Commun. 49 (2013) 3327–3329.

[21] Y. Huang, H. Ma, S. Wang, M. Shen, R. Guo, X. Cao, M. Zhu, X. Shi, Efficient catalytic reduction of hexavalent chromium using palladium nanoparticle-immobilized electrospun polymer nanofibers, ACS Appl. Mater. Interfaces 4 (2012) 3054–3061.

[22] M.A. Omole, I.O. K'Owino, O.A. Sadik, Palladium nanoparticles for catalytic reduction of Cr(VI) using formic acid, Appl. Catal. B: Environ. 76 (2007) 158–167.

[23] K. Gong, W. Wang, J. Yan, Z. Han, Highly reduced molybdophosphate as a noble metal-free catalyst for the reduction of chromium using formic acid as a reducing agent, J. Mater. Chem. A 3 (2015) 6019–6027.

[24] H.-T. Ren, S.-Y. Jia, J.-J. Zou, S.-H. Wu, X. Han, A facile preparation of Ag_2O/P25 photocatalyst for selective reduction of nitrate, Appl. Catal. B: Environ. 176–177 (2015) 53–61.

[25] O.S.G.P. Soares, M.F.R. Pereira, J.J.M. Órfão, J.L. Faria, C.G. Silva, Photocatalytic nitrate reduction over Pd–Cu/TiO_2, Chem. Eng. J. 251 (2014) 123–130.

[26] R.M. Mohamed, E.S. Baeissa, Environmental remediation of aqueous nitrate solutions by photocatalytic reduction using Pd/$NaTaO_3$ nanoparticles, J. Ind. Eng. Chem. 20 (2014) 1367–1372.

[27] I. Dodouche, F. Epron, Promoting effect of electroactive polymer supports on the catalytic performances of palladium-based catalysts for nitrite reduction in water, Appl. Catal. B: Environ. 76 (2007) 291–299.

[28] M.B. Gawande, P.S. Branco, R.S. Varma, Nano-magnetite (Fe_3O_4) as a support for recyclable catalysts in the development of sustainable methodologies, Chem. Soc. Rev. 42 (2013) 3371–3393.

[29] X. Pan, Y.-J. Xu, Efficient thermal and photocatalyst of Pd nanoparticles on TiO_2 achieved by an oxygen vacancies promoted synthesis strategy, ACS Appl. Mater. Interfaces 6 (2014) 1879–1886.

[30] R. Li, P. Zhang, Y. Huang, C. Chen, Q. Chen, Facile approach to prepare Pd nanoarray catalysts within porous alumina templates on macroscopic scales, ACS Appl. Mater. Interfaces 5 (2013) 12695–12700.

[31] D.S. Su, S. Perathoner, G. Centi, Nanocarbons for the development of advanced catalysts, Chem. Rev. 113 (2013) 5782–5816.

[32] H. Chang, H. Wu, Graphene-based nanocomposites: preparation, functionalization, and energy and environmental applications, Energy Environ. Sci. 6 (2013) 3483–3507.

[33] L. Ren, F. Yang, C. Wang, Y. Li, H. Liu, Z. Tu, L. Zhang, Z. Liu, J. Gao, C. Xu, Plasma synthesis of oxidized graphene foam supporting Pd nanoparticles as a new catalyst for one-pot synthesis of dibenzyls, RSC Adv. 4 (2014) 63048–63054.

[34] K. Mori, M. Dojo, H. Yamashita, Pd and Pd-Ag nanoparticles within a macroreticular basic resin: an efficient catalyst for hydrogen production from formic acid decomposition, ACS Catal. 3 (2013) 1114–1119.

[35] A.M. Trzeciak, E. Mieczyńska, J.J. Ziółkowski, W. Bukowski, A. Bukowska, J. Noworól, J. Okal, Palladium(0) nanoparticles encapsulated in diamine-modified glycidyl methacrylate polymer (GMA-CHDA) applied as catalyst of Suzuki–Miyaura cross-coupling reaction, New J. Chem. 32 (2008) 1124–1130.

[36] J. Huang, D. Wang, H. Hou, T. You, Electrospun palladium nanoparticle-loaded carbon nanofibers and their electrocatalytic activities towards hydrogen peroxide and NADH, Adv. Funct. Mater. 18 (2008) 441–448.

[37] M.M. Demir, M.A. Gulgun, Y.Z. Menceloglu, B. Erman, S.S. Abramchuk, E.E. Makhaeva, A.R. Khokhlov, V.G. Matveeva, M.G. Sulman, Palladium nanoparticles by electrospinning from poly(acrylonitrile-co-acrylic acid)-$PdCl_2$ solutions: relations between preparation conditions, particle size, and catalytic activity, Macromolecules 37 (2004) 1787–1792.

[38] F. Hapiot, S. Menuel, E. Monflier, Thermoresponsive hydrogels in catalysis, ACS Catal. 3 (2013) 1006–1010.

[39] A. Desforges, R. Backov, H. Deleuze, O. Mondain-Monval, Generation of palladium nanoparticles within macrocellular polymeric supports: application to heterogeneous catalysis of the Suzuki-Miyaura coupling reaction, Adv. Funct. Mater. 15 (2005) 1689–1695.

[40] A. Alonso, A. Shafir, J. Macanás, A. Vallribera, M. Muñoza, D.N. Muraviev, Recyclable polymer-stabilized nanocatalysts with enhanced accessibility for reactants, Catal. Today 193 (2012) 200–206.

[41] Y.Y.N. Bonggotgetsakul, R.W. Cattrall, S.D. Kolev, A method for coating a polymer inclusion membrane with palladium nanoparticles, React. Funct. Polym. 97 (2015) 30–36.

[42] M. Zeng, X. Yuan, Z. Yang, C. Qi, Novel macroporous palladium cation crosslinked chitosan membranes for heterogeneous catalysis application, Int. J. Biol. Macromol. 68 (2014) 189–197.

[43] K. Soukup, P. Topka, V. Hejtmánek, D. Petráš, V. Valeš, O. Šolcová, Noble metal catalysts supported on nanofibrous polymeric membranes for environmental applications, Catal. Today 236 (2014) 3–11.

[44] E. Hariprasad, T.P. Radhakrishnan, Palladium nanoparticle-embedded polymer thin film dip catalyst for Suzuki–Miyaura reaction, ACS Catal. 2 (2012) 1179–1186.

[45] V.W. Faria, D.G.M. Oliveira, M.H.S. Kurz, F.F. Gonçalves, C.W. Scheeren, G.R. Rosa, Palladium nanoparticles supported in a polymeric membrane: an efficient phosphine-free green catalyst for Suzuki–Miyaura reactions in water, RSC Adv. 4 (2014) 13446–13452.

[46] M. Nasrollahzadeh, S.M. Sajadi, A. Hatamifard, Waste chicken eggshell as a natural valuable resource and environmentally benign support for biosynthesis of catalytically active Cu/eggshell, Fe_3O_4/eggshell and Cu/Fe_3O_4/eggshell nanocomposites, Appl. Catal. B: Environ. 191 (2016) 209–227.

[47] M. Liang, R. Su, W. Qi, Y. Zhang, R. Huang, Y. Yu, L. Wang, Z. He, Reduction of hexavalent chromium using recyclable Pt/Pd nanoparticles immobilized on procyanidin-grafted egg shell membrane, Ind. Eng. Chem. Res. 53 (2014) 13635–13643.

[48] S. Chappa, R.N. Shinde, A.K. Pandey, Self-reducing asymmetric polymer membrane for in situ formation and containment of noble metal nanocatalysts, Green Chem. 17 (2015) 4157–4161.

[49] C. Agarwal, A.K. Pandey, S. Chaudhury, V.T. Aher, A.K. Patra, P.U. Sastry, A. Goswami, Ionic transport in polyelectrolyte-filled cation-exchange membranes, J. Membr. Sci. 446 (2013) 125–131.

[50] V.C. Adya, A. Sengupta, S.K. Thulasidas, V. Natarajan, Exploration of CCD-based ICP-AES for studying spectral interferences of uranium on other analytes, At. Spectrosc. 37 (2016) 19–24.

[51] C. Agarwal, A.K. Pandey, S. Das, M.K. Sharma, D. Pattyn, P. Ares, A. Goswami, Neck-size distributions of through-pores in polymer membranes, J. Membr. Sci. 415–416 (2012) 608–615.

[52] D.V. Goia, E. Matijević, Preparation of monodispersed metal particles, New J. Chem. 22 (1998) 1203–1215.

[53] B. Gralec, A. Lewera, Catalytic activity of unsupported Pd-Pt nanoalloys with low Pt content towards formic acid oxidation, Appl. Catal. B: Environ. 192 (2016) 304–310.

[54] N. Misbah, I.N. Iftikhar, Synthesis, spectral and electrochemical studies of complex of uranium(IV) with pyridine-3-carboxylic acid, Am. J. Anal. Chem. 4 (2013) 134–140.

[55] S.J. Azizian, Kinetic models of sorption: a theoretical analysis, Colloid Interface Sci. 276 (2004) 47–52.

[56] S. Das, A.K. Pandey, A.A. Athawale, V.K. Manchanda, Exchanges of uranium(VI)-species in amidoxime functionalized sorbents, J. Phys. Chem. B 113 (2009) 6329–6335.

[57] H. Xu, B.W. Zeiger, K.S. Suslick, Sonochemical synthesis of nanomaterials, Chem. Soc. Rev. 42 (2013) 2555–2567.

[58] Y.G. Adewuyi, Sonochemistry: environmental science and engineering applications, Ind. Eng. Chem. Res. 40 (2001) 4681–4715.

[59] S.I. Nikitenko, L. Venault, R. Pflieger, T. Chave, I. Bisel, P. Moisy, Potential applications of sonochemistry in spent nuclear fuel reprocessing: a short review, Ultrason. Sonochem. 17 (2010) 1033–1040.